Inorganic Chemistry

Article

pubs.acs.org/IC

Modeling the Active Site of [NiFe] Hydrogenases and the [NiFe$_u$] Subsite of the C-Cluster of Carbon Monoxide Dehydrogenases: Low-Spin Iron(II) Versus High-Spin Iron(II)

Katharina Weber, Özlen F. Erdem, Eckhard Bill, Thomas Weyhermüller, and Wolfgang Lubitz*

Max Planck Institute for Chemical Energy Conversion, Stiftstrasse 34-36, D-45470 Mülheim an der Ruhr, Germany

Supporting Information

ABSTRACT: A series of four [S_2Ni(μ-S)$_2$FeCp*Cl] compounds with different tetradentate thiolate/thioether ligands bound to the Ni(II) ion is reported (Cp* = C_5Me_5). The {S_2Ni(μ-S)$_2$Fe} core of these compounds resembles structural features of the active site of [NiFe] hydrogenases. Detailed analyses of the electronic structures of these compounds by Mössbauer and electron paramagnetic resonance spectroscopy, magnetic measurements, and density functional theory calculations reveal the oxidation states Ni(II) low spin and Fe(II) high spin for the metal ions. The same electronic configurations have been suggested for the C_{red1} state of the C-cluster [NiFe$_u$] subsite in carbon monoxide dehydrogenases (CODH). The Ni−Fe distance of ∼3 Å excludes a metal−metal bond between nickel and iron, which is in agreement with the computational results. Electrochemical experiments show that iron is the redox active site in these complexes, performing a reversible one-electron oxidation. The four complexes are discussed with regard to their similarities and differences both to the [NiFe] hydrogenases and the C-cluster of Ni-containing CODH.

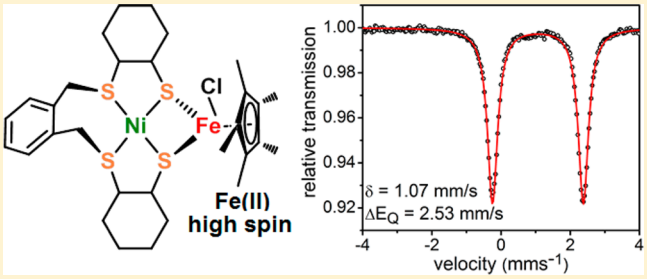

INTRODUCTION

Nickel and iron are found in the active sites of numerous enzymes with different functionality. Metalloenzymes containing a combined [NiFe] subsite are involved in the biological conversion of hydrogen, carbon monoxide, and carbon dioxide.[1] [NiFe], [FeFe], and [Fe] hydrogenases belong to a class of metalloenzymes that function in biological energy metabolism as catalysts for the reversible oxidation of hydrogen to protons and electrons.[2,3] Since the elucidation of the [NiFe] hydrogenase enzyme structure by Volbeda et al. in 1995 the active heterobimetallic [NiFe] cluster is known to be anchored in the protein by two terminal cysteine residues and two bridging cysteines connecting the metal ions (Figure 1a).[4,5] Essentially only the sulfur-coordinated nickel is involved in the redox processes responsible for hydrogen conversion, as was confirmed by electron paramagnetic resonance (EPR) spectroscopy,[6] whereas the ferrous ion is best described as low-spin Fe(II) (S = 0) throughout the catalytic cycle based on Mössbauer spectroscopy.[7,8] The low-spin state of iron is caused by a set of strong ligands, identified by Fourier transform infrared spectroscopy as two CN^- and one CO.[9] Using a variety of spectroscopic techniques, different redox states of the active site were identified.[10−12] In spite of the basic redox-inactivity of iron, both metals were found to be influenced by redox steps presumably due to changes in the nature of the chemical bonds of the ligands and electronic interaction between the metal centers.[7,13,14]

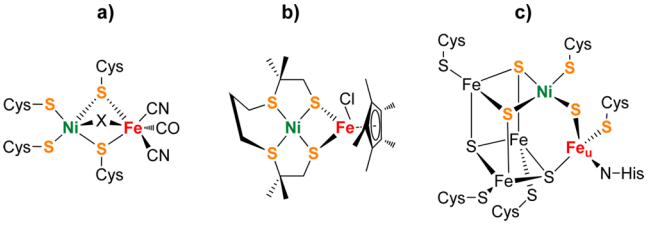

Figure 1. (a) Active site of [NiFe]-hydrogenases; (b) [NiFe]-model complex; (c) Reduced, active form of CODH C-cluster.

Modeling the active site of [NiFe] hydrogenases has been of interest for bioinorganic chemists with the perspective of developing cheap hydrogen-producing catalysts.[3,15−19] However, synthesis of an asymmetric [NiFe] core is challenging, and the number of small-molecule models that truly incorporate one iron and one nickel ion is low compared to the number of [FeFe] hydrogenase models available now. Although some models exhibit remarkable resemblance to the active site,[20−22] most of the previously reported dinuclear models reproduce only certain structural features.[23−31] So far, only a few dinuclear [NiFe] compounds have been reported to exhibit also functional electrocatalytic activity toward proton reduction or hydrogen oxidation.[32−37] All models reported so far have in common that the iron atom is in the low-spin state, caused by strong π-accepting ligands like carbonyl, nitric oxide, or phosphites, similar to the active site of [NiFe] hydrogenases

Received: April 23, 2014
Published: June 6, 2014

   dx.doi.org/10.1021/ic500910z | Inorg. Chem. 2014, 53, 6329−6337

Scheme 1. Synthesis of Compounds 1−4[a]

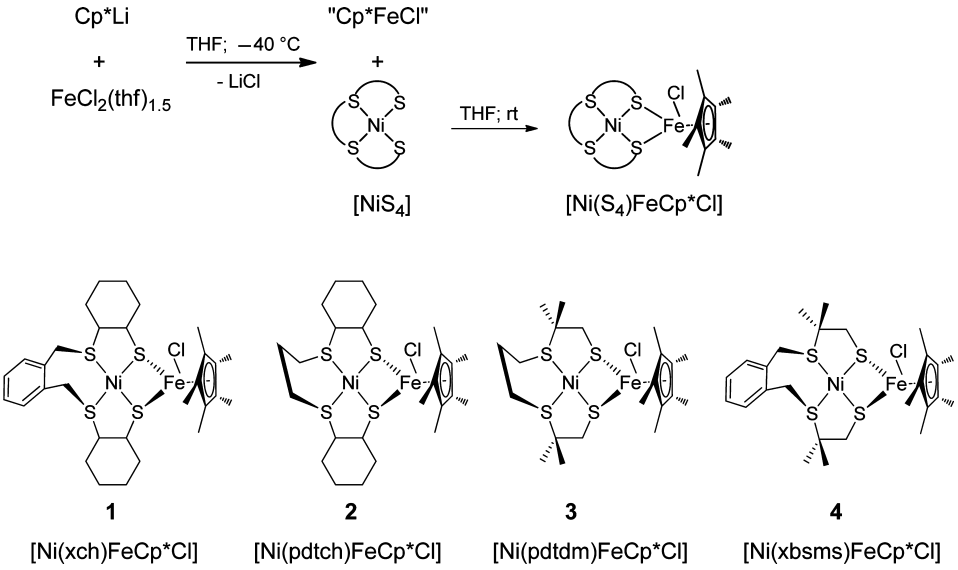

[a](H_2xch = α,α'-bis(*trans*-2-mercapto-1-thiacyclohexyl)-*o*-xylene, H_2pdtch = 1,3-bis(*trans*-2-mercapto-1-thiacyclohexyl)propane, H_2pdtdm = 1,9-dimercapto-3,7-dithia-2,2,8,8-tetramethylnonane, H_2xbsms = α,α-bis(4-mercapto-3,3-methyl-2-thiabutyl)-*o*-xylene).

that bear strong-field ligands on the iron site. Therefore, it seems likely that the particular electronic structure of the iron center in the active site plays an important role for the functionality of the enzyme as nature also took the challenge to bring the biologically unusual and toxic CO and CN^- ligands into position for this system.

A [NiFe] subsite is also found in the C-cluster of Ni-containing carbon monoxide dehydrogenases (CODH), which belong to a class of metalloenzymes that catalyze the reversible oxidation of CO to CO_2, a process with a central role in the global carbon cycle.[38,39] The C-cluster consists of an $[Fe_3S_4]$ unit linked to a $[NiFe_u]$ subsite with a sulfur-only coordinated, square-planar nickel atom and a unique Fe_u site, called ferrous component II (FCII), with a distorted tetrahedral geometry (Figure 1c).[40−42] The bridging sulfide between nickel and iron is exchangeable, for instance, by hydroxide.[40] Different redox states of the C-cluster can be stabilized, of which only the C_{red1} state is assumed to react with CO during catalysis.[43] From Mössbauer studies, the unique iron atom Fe_u in C_{red1} was identified as high-spin Fe(II), and the nickel is assigned as low-spin Ni(II) from X-ray absorption spectroscopy results.[44−46] Though the mechanism is still controversial, there is agreement that both the nickel and the unique iron in the cluster are crucial for the catalytic activity of the enzyme. A series of structural models mimicking the cuboidal mixed-metal C-cluster were reported by Holm et al.[47−52] Some of them reproduce the square planar geometry expected for the low-spin Ni(II). However, all models are lacking the noncuboidal unique exo-Fe center, which is difficult to implement within such clusters.

In this work we report synthesis and characterization of a series of $\{S_2Ni(\mu\text{-}S)_2FeCp^*Cl\}$ complexes (Cp* = pentamethylcyclopentadienyl). The butterfly-shaped $\{S_2Ni(\mu\text{-}S)_2Fe\}$ core is characteristic of the active site of [NiFe] hydrogenases, whereas the unusual electronic configuration with low-spin Ni(II) and high-spin Fe(II) resembles that of the $[NiFe_u]$ subsite in the C_{red1} state of the CODH C-cluster. Therefore, the presented series of bioinorganic model compounds is discussed in comparison both to the [NiFe] hydrogenases and to the C-cluster of Ni-containing CODH.

RESULTS

Synthesis. The heterobimetallic compounds **1**−**4** were synthesized by reaction of Cp*FeCl, prepared *in situ* from Cp*Li and $FeCl_2(THF)_{1.5}$,[53] with the corresponding NiS_4 precursor compound in tetrahydrofuran (THF) under an inert atmosphere (Scheme 1). To suppress the formation of undesirable homometallic thiolate clusters, different tetradentate thiolate/thioether ligands were used on the nickel site.[54,55] Resulting LiCl was removed by filtration, and dark red crystals of **1**−**4** were obtained by layering the reaction solution with *n*-hexane. The isolated solids are stable at room temperature under inert atmosphere. The reactivity of compounds **1**−**4** was tested on compound **1** as a representative of this series. A THF solution of **1** changed the color from red to brown after saturation with CO gas. However, upon solvent evaporation an off-white powder started to precipitate indicating a decomposition of the complex. Furthermore, the addition of a hydride source ($LiBEt_3H$ or $LiAlH_4$) to a THF solution of **1** at −40 °C yielded a dark brown solution from which no product could be isolated and identified. Finally, no reaction was observed under hydrogen atmosphere.

Structural Characterization. Single-crystal X-ray structure determinations were performed for all compounds **1**−**4**. Crystallographic details are listed in Table S1 in the Supporting Information, molecular structure representations are shown in Figure 2, and selected bond distances and angles are listed in Table 1.

The structures of **1**−**4** contain square planar NiS_4 cores bound to a [FeCp*Cl] unit via two bridging thiolate donors. The NiS_4 fragment of the diamagnetic, square planar starting compounds, formed by the four sulfur atoms of the thioether and thiolate functions of the chelating ligands, is conserved in all four [NiFe] complexes as also observed in other [NiFe] and [NiRu] structures reported in the literature.[28,34,56,57] Dihedral angles (NiS1S2/NiS3S4) of 2.81−5.73° are observed, indicat-

dx.doi.org/10.1021/ic500910z | Inorg. Chem. 2014, 53, 6329−6337

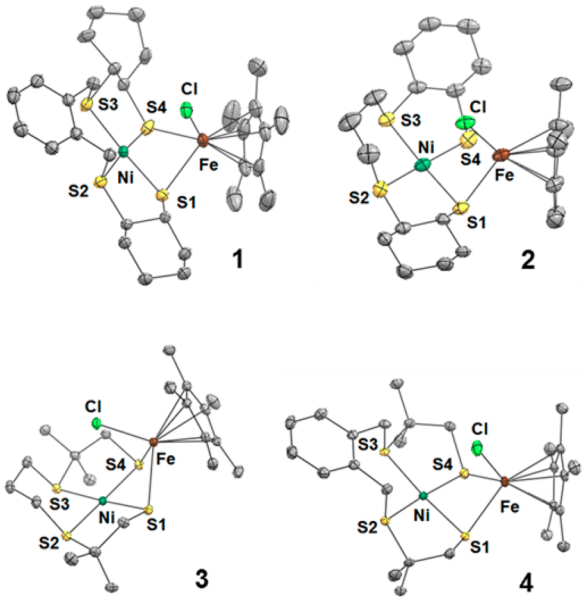

Figure 2. Molecular structures of compounds **1**−**4**. Thermal ellipsoids are shown at the 50% probability level. Hydrogen atoms and most carbon labels are omitted for clarity.

ing a small tetrahedral distortion of the NiS_4 moiety. The Ni−S bond lengths are slightly longer than they are in the corresponding NiS_4 precursors.[54,55] While in [NiFe] hydrogenases the nickel is in a strongly distorted square pyramidal conformation,[4] in the reduced state of the CODH C-cluster a slightly tetrahedrally distorted square planar geometry around nickel is found with Ni−S bond lengths of ∼2.3 Å.[40] In molecular structures of **1**−**4** a pseudotetrahedral coordination sphere around the iron atom is formed by two bridging thiolates, a pentamethylcyclopentadienyl anion, and a chloride. Remarkably, the Fe−S bond lengths of 2.45−2.51 Å are significantly longer than those observed in other [Ni(μ-S)$_2$Fe] complexes (2.1−2.3 Å).[29,34] Furthermore, the Fe−Cp* centroid distance in **1**−**4** is about 0.25 Å longer than it is in the diamagnetic complex [FeCp*(dppe)Cl].[58] The long iron−ligand distances indicate that the iron centers in compounds **1**−**4** are presumably in the high-spin state. This is remarkable since very few high-spin cyclopentadienyl complexes of iron(II) have been reported in the literature.[59−61] To the best of our knowledge, no examples have been reported in the literature with {FeCp*} fragments that were identified and assigned to the Fe(II) high-spin state.

All complexes reveal a relatively long metal−metal distance around 3 Å, excluding a bonding interaction between the metals, which was observed in model compounds with Ni−Fe distances of around 2.5 Å.[29,35] In different structures of [NiFe] hydrogenases, determined by X-ray crystallography, the metal−metal separation varies from 2.53 Å up to 3.23 Å, depending on the redox state of the enzyme, with longer distances assigned to the oxidized forms of the enzyme.[29] In the C-cluster of CODH, a Ni−Fe_u distance of 2.8−2.9 Å was determined.[40] The [Ni(μ-S)$_2$Fe] motif is V-shaped with dihedral angles of 61° to 71° (NiS1S4/FeS1S4) showing a change in geometry of the butterfly unit with varying NiS_4 fragment. In different structures of [NiFe] hydrogenases a high flexibility of the butterfly pattern in different redox states is observed with the dihedral angle between the NiSS and FeSS planes varying in the range of 46° to 99°.[29]

Electronic Structure. Solutions of compounds **1**−**4** are paramagnetic, which obstructs detection of well-resolved NMR spectra. For a quantitative magnetic susceptibility study superconducting quantum interference device (SQUID) measurements were performed on solid samples in the temperature range of 2−300 K (Figure 3). Above 100 K all

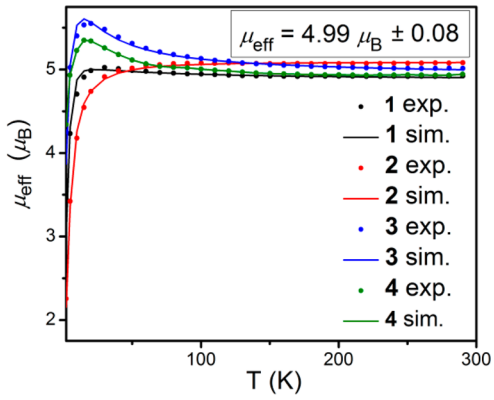

Figure 3. Temperature dependence of the solid-state effective magnetic moment μ_{eff} of compounds **1**−**4**. The dots correspond to experimental data. The solid lines are spin-Hamiltonian simulations (Supporting Information, Table S2).

four complexes **1**−**4** showed similar, essentially constant effective magnetic moments of 4.99 ± 0.08 μ_B. The data are close to the spin-only value of 4.90 μ_B expected for the isolated-spin S = 2 in the high-temperature limit.[62] The paramagnetism cannot be assigned to the Ni(II) centers because the square

Table 1. Selected Bond Distances (Å) and Angles in Compounds 1−4

	1	2	3	4
Ni−Fe	2.9810(6)	3.0685(6)	3.0957(5)	3.0903(4)
Ni−S1	2.1807(7)	2.1824(8)	2.1822(5)	2.1884(5)
Ni−S2	2.1957(8)	2.194(1)	2.1907(5)	2.2059(5)
Ni−S3	2.2067(7)	2.1928(9)	2.1966(5)	2.2207(5)
Ni−S4	2.1790(8)	2.192(1)	2.1907(5)	2.1731(4)
Fe−S1	2.5106(8)	2.4791(8)	2.5051(6)	2.4712(5)
Fe−S4	2.4670(8)	2.4494(7)	2.4969(5)	2.4542(5)
Fe−Cl	2.3149(9)	2.3497(9)	2.3283(5)	2.3361(5)
Fe−Cp*(centroid)	2.007	2.029	2.023	2.014
NiS1S2/NiS3S4	2.99°	5.73°	3.63°	2.81°
NiS1S4/FeS1S4	70.88°	61.28°	61.69°	62.25°

dx.doi.org/10.1021/ic500910z | Inorg. Chem. 2014, 53, 6329−6337

planar coordination geometries afford a low-spin $S = 0$ state for the $3d^8$ configuration. Thus, the effective moments clearly reveal high-spin ground states of the Fe(II) ions ($S = 2$) in all compounds **1**–**4**. The corresponding high-spin $3d^6$ configuration of Fe(II) is expected to show a decline of $\mu_{eff}(T)$ at low temperatures due to zero-field splitting (ZFS) arising from spin–orbit coupling of ground and excited states.[62]

For complex **2** the decrease of μ_{eff} is indeed observed in the low-temperature range, as expected, and the data can be nicely fitted by using the usual spin-Hamiltonian description for a mononuclear $S = 2$ system with axial and rhombic ZFS parameters $D = 16$ cm^{-1} and $E/D = 0.11$ (see Supporting Information).[62] The effective magnetic moments of complexes **1**, **3**, and **4**, however, exhibit maxima at 15–30 K instead of just monotonous decrease. These peaks cannot be assigned to spin–orbit coupling or another single-ion property, but are characteristic of weak ferromagnetic coupling, superimposed on the effect of ZFS.[62] Since the nickel ions are diamagnetic, only an intermolecular interaction of neighboring Fe(II) ions in the solid structure can be the reason for this phenomenon. Approximate simulations of the effect can be achieved with a two-spin coupling term, $2JS_1 \cdot S_2$, as a crude hypothetical model of weak 2D or 3D interactions in the real solids (see Supporting Information). The simulations shown in Figure 3 yield reasonable estimates for the interaction with coupling constants J in the range from +0.65 to +1.65 cm^{-1} (Supporting Information, Table S2). As a consequence of this spin coupling the zero-field parameters D and E/D of **1**, **3**, and **4** cannot be reliably determined from magnetic susceptibility data; one may even doubt whether the data for **2** are fully reliable. The best values of the ZFS parameters obtained with a hypothetical dimer coupling included in the simulations are found in the range of 11 and 16 cm^{-1} (Supporting Information, Table S2, with ca. 30–50% uncertainty). Values of similar magnitude are found for Fe(II) high-spin centers in synthetic compounds and in proteins.[63−65]

Interestingly, ferromagnetic intermolecular spin coupling was also observed in THF solution of compound **1**, for which SQUID measurements were undertaken as representative of the whole series (Supporting Information, Figure S1). Apparently the molecules tend to aggregate also in solution. Nevertheless, X-band continuous wave (CW) EPR spectra could be recorded for compound **1** in frozen THF solution at 10 K with the microwave magnetic field $\mathbf{B}_1$ taken parallel and perpendicular to the static field $\mathbf{B}_0$, as shown in Supporting Information, Figure S2. A typical broad integer-spin signal was observed in conventional (perpendicular) detection-mode, whereas with parallel-mode polarization additional sharp features have been resolved.[66] By means of EPR spectroscopy, high-spin iron species were identified previously in synthetic transition metal complexes and biological systems at X-band frequencies ($h\nu \approx 0.3$ cm^{-1}) under the condition that the axial ZFS parameter is small enough to allow for non-Kramers transitions in the spin manifold.[67−74] Because of the intermolecular coupling of compound **1**, we suggest that the EPR signals in our case arise from spin-coupled magnetic states, which partially can have very small contributions from single-ion ZFS due to vanishing spin-projection factors.[75] Unfortunately the spectra can therefore not provide D and E/D for the individual Fe(II) sites.

The high-spin $S = 2$ ground state of Fe(II) is readily confirmed by ^{57}Fe Mössbauer spectroscopy. Zero-field Mössbauer spectra of solid **1**–**4** at 80 K exhibit quadrupole doublets with isomer shifts in the range of $\delta = 0.96$–1.08 mm/s and quadrupole splittings of $\Delta E_Q = 2.53$–2.63 mm/s (Figure 4). The high isomer shifts around 1 mm/s are unique for high-spin iron(II), and the observed moderately large quadrupole splittings are consistent with the corresponding $t_{2g}^4 e_g^2$ configuration.[76] The Mössbauer parameters were correctly predicted by DFT calculations, as shown in Table 2.[77] Computational details are given in the Supporting Information. In a previous Mössbauer study on different redox states of the C-cluster of CODH Münck and co-workers identified the unique exo-iron of the cluster (Fe_u) to be high-spin Fe(II). Its characteristic Mössbauer parameters $\delta = 0.82$ mm/s and $\Delta E_Q = 2.82$ mm/s are remarkably close to those found here for complexes **1**–**4**.[44]

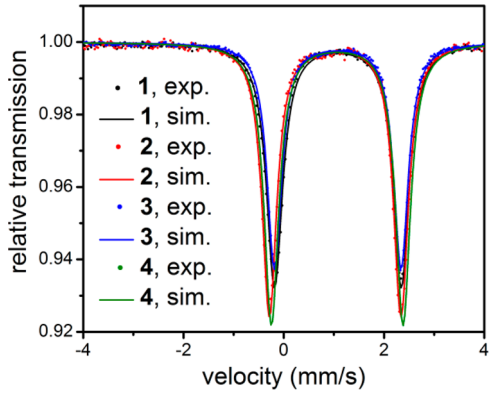

Figure 4. Mössbauer spectra of **1**–**4** recorded at 80 K without an applied external field and fits with Lorentzian doublets (colored lines). Resulting Mössbauer parameters are given in Table 2

Electrochemical Characterization. The electrochemical properties of complexes **1**–**4** were investigated using cyclic voltammetry in THF solution (1 mM) at scan rates of 100–1000 mV/s with NBu_4PF_6 (0.2 M) as supporting electrolyte. All four compounds show one reversible one-electron redox wave with very similar potentials at −0.88 to −0.91 V vs Fc/Fc$^+$ and similar E_{pa} and E_{pc} peak separations (~90 mV at a scan rate of 100 mV/s, $i_{pa}/i_{pc} \approx 1$, irrespective of the scan rate), indicating that changes in the coordination sphere of nickel do not have a significant impact on the redox behavior of the compounds. Furthermore, the NiS_4 precursors were reported to exhibit only irreversible electrochemical behavior.[54,55] Therefore, we can deduce that iron is the redox-active metal in these compounds, in contrast to the situation found for the active site of [NiFe] hydrogenases. The reversible redox transition is attributed to the Fe(II)/Fe(III) redox couple, since the reduction of an electron-rich Fe(II) center in this potential range is unlikely. No catalytic activity in electrochemical proton reduction could be observed for complexes **1**–**4**; in contrast, addition of acid leads to immediate decomposition of the compounds. The cyclic voltammograms recorded at various scan rates with complex **1** as a representative for this series are shown in Figure 5. The redox properties of compounds **1**–**4** are listed in Table 3.

Density-Functional Computations. DFT calculations were performed to obtain more insight into the electronic structure of complex **1** as a representative for this series of compounds. Unconstrained geometry relaxations were performed for the quintet using the BP86 functional starting from the available crystal structure. A comparison of optimized metrical parameters with the experimental values is given in the

dx.doi.org/10.1021/ic500910z | Inorg. Chem. 2014, 53, 6329–6337

Table 2. Experimental and Calculated (B3LYP/CP(PPP)) Mössbauer Parameters for 1−4

parameter	1, exp.[a]	1, calc.	2, exp.[a]	2, calc.	3, exp.[a]	3, calc.	4, exp.[a]	4, calc.
δ [mm/s]	1.07	0.97	0.96	0.94	1.08	0.97	1.07	0.95
ΔE_Q [mm/s]	2.53	2.58	2.68	2.87	2.53	2.69	2.63	2.73

[a]Zero field at 80 K.

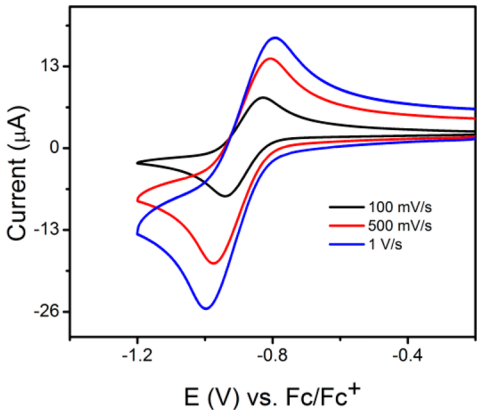

Figure 5. Cyclic voltammogram of **1** in THF (1 mmol L^{-1}) recorded at scan rates of 100 to 1000 mV/s with NBu_4PF_6 (0.2 M) as supporting electrolyte.

Table 3. Electrochemical Data of 1−4

compound	$E_{1/2}$ (mV)[a]	ΔE_p (mV)[a]
[Ni(xch)FeCp*Cl] **1**	−907	96
[Ni(pdtch)FeCp*Cl] **2**	−895	90
[Ni(pdtdm)FeCp*Cl] **3**	−882	88
[Ni(xbsms)FeCp*Cl] **4**	−910	86

[a]In THF (1 mmol/L) recorded at scan rates of 100 mV/s with NBu_4PF_6 (0.2 M) as supporting electrolyte. All potentials are referred to the Fc/Fc^+ redox couple.

Supporting Information (Table S3). The starting geometry relaxes with a slight bond elongation of all Ni−S bonds and an increase of the tetrahedral distortion around the nickel atom upon optimization. Unrestricted single-point calculations were performed at the optimized structure using the hybrid B3LYP functional and a relativistically recontracted basis set (def2-TZVP) on all atoms. The quintet state ($S = 2$) was found to be 19.5 kcal/mol lower in energy than the closed-shell singlet ($S = 0$). Figure 6 illustrates the calculated total spin density, which is mainly located on iron (87% according to Mulliken spin-population analysis) without significant delocalization onto the nickel ion. The calculated spin-expectation value $\langle \hat{S}^2 \rangle$ is nearly equal to the ideal value $S(S + 1) = 6$ for $S = 2$ so that compound **1** can be treated as an almost "pure" spin system. As explained by Neese et al., so-called quasi-restricted orbitals

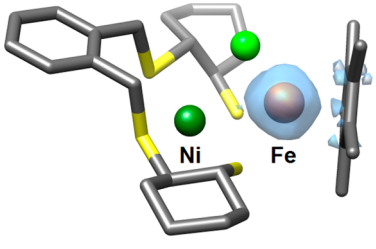

Figure 6. Calculated spin density (pale blue) plot of complex **1**.

(QROs) are well-suited for a qualitative visualization of the calculated frontier molecular orbitals.[78,79] In the set of QROs five molecular orbitals (MOs) with major contributions from iron d orbitals are found (Figure 7). The degeneracy of d

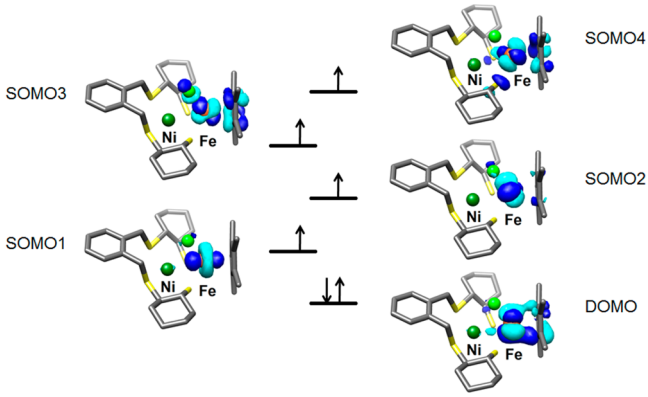

Figure 7. Qualitative MO scheme of **1** based on calculated quasi-restricted orbitals.

orbitals is fully omitted giving rise to one doubly occupied molecular orbital (DOMO) and four singly occupied molecular orbitals (SOMOs), consistent with the high-spin Fe(II) ($3d^6$, $S = 2$) state as also derived from experimental results. The DOMO reveals a π-bonding interaction of an iron-centered d orbital to the Cp^{*-} ligand. The energetically highest SOMO4 has antibonding character between iron and the sulfurs, thus explaining the significantly longer Fe−S bonds observed in the structures of complexes **1**−**4** compared to the analogous low-spin [NiFe] complexes reported in the literature.[29,34] No bonding interaction between nickel and iron is predicted in contrast to other [NiFe] models containing a nickel−iron σ bond.[29,35] Altogether, the calculated electronic structure is in agreement with the experimental data and confirms the assumption of a low-spin Ni(II) and a high-spin Fe(II) configuration in the complexes **1**−**4**.

DISCUSSION

Our results classify complexes **1**−**4** as model compounds for [NiFe] hydrogenases with respect to the structure of the active site and for the C-cluster of carbon monoxide dehydrogenases with respect to the electronic structure of the $[NiFe_u]$ subsite. In these two enzymes, nature uses the same metals, nickel and iron, but implements them in the active site with completely different electronic properties. In [NiFe] hydrogenases, nature takes the challenge of installing biotoxic strong-field ligands CO (π-backbonding) and CN^- (σ-donating and π-backbonding) at the iron site. This ligand set conserves the iron in the low-spin state with a variable electron density, which enables it to compensate the electronic changes on the redox-active nickel via electronic interaction between the metal centers. However, in the C-cluster a tetrahedral geometry around the unique iron site enables the cluster to achieve the Fe(II) high-spin state, and, at the same time, a CO coordination, which would lead to

dx.doi.org/10.1021/ic500910z | Inorg. Chem. 2014, 53, 6329−6337

a low-spin state of iron, is avoided. Taking into account that CO is a substrate of CODH, the importance of the high-spin state of iron for reactivity becomes obvious. Instead, CO is assumed to bind to nickel in the catalytic cycle of CODH.[43] In complexes **1**−**4** the electronic structure was clearly assigned as low-spin Ni(II) and high-spin Fe(II) by Mössbauer spectroscopy, magnetic susceptibility measurements, and DFT calculations. The electronic structure is also reflected in the molecular structures of these compounds:

(1) the nickel coordination geometry is square planar, in analogy to the [$NiFe_u$]-subsite of CODH;
(2) the pseudotetrahedral coordination sphere at the iron site contains Fe−S bonds that are longer than those observed for other [$Ni(\mu\text{-}S)_2Fe$] complexes with low-spin iron;
(3) the Fe−Cp* centroid distance is significantly longer than it is in the mononuclear low-spin compound [FeCp*(dppe)Cl];
(4) Ni−Fe distances of ∼3 Å are found in the molecular structures of **1**−**4** excluding the presence of a metal−metal bond.

In the C-cluster of CODH a Ni−Fe_u distance of 2.8−2.9 Å was determined, suggesting that a metal−metal bond between nickel and the unique iron probably is not present in the C_{red1} state of CODH, similar to the model compounds **1**−**4**. It is more feasible that they are just positioned close to each other by the associated cuboidal cluster. While the redox behavior of Ni and Fe_u in the C-cluster of CODH is still controversial, in [NiFe] hydrogenases the nickel ion was identified to be redox-active, and iron remains low-spin Fe(II). Complexes **1**−**4** undergo a reversible one-electron oxidation on iron at mild potentials but do not exhibit a reversible reduction. In contrast to the diamagnetic complex [$S_2Ni(\mu\text{-}S)_2FeCpCO$], which was reported by Artero et al. and was found to be active in electrocatalytic proton reduction,[34] complexes of this series are paramagnetic and decompose upon addition of acid. This accentuates the importance of the carbonyl ligand in the active site of [NiFe] hydrogenases to yield a low-spin state of the iron center.

CONCLUSIONS

A series of new [$S_2Ni(\mu\text{-}S)_2FeCp^*Cl$] complexes related to the [NiFe] hydrogenase active site and the [$NiFe_u$] subsite of the C-cluster in CODH was synthesized and characterized. Molecular structures of **1**−**4** reveal a square planar geometry around the Ni(II) ion and a pseudotetrahedral geometry around iron. The electrochemical behavior of the reported model complexes indicates iron as the redox-active center with a reversible one-electron oxidation. In contrast, in [NiFe] hydrogenases nickel is the redox-active metal and is electronically supported by the low-spin iron. ^{57}Fe Mössbauer spectroscopy as well as SQUID data reveal that complexes **1**−**4** are paramagnetic and contain a high-spin Fe(II) coordinated to a low-spin Ni(II)S_4 fragment. The calculated spin-density distribution clearly identifies iron as the paramagnetic center without significant electronic interaction between the metal ions. Furthermore, DFT calculations reveal that the quintet-state is significantly lower in energy than the closed-shell singlet (19.5 kcal/mol for compound **1**), thus indicating a small ligand-field splitting. The low-spin Ni(II)/high-spin Fe(II) electronic configuration resembles the [$NiFe_u$] subsite in the C_{red1} state of the C-cluster in CODH, which was shown to play a key role in the catalytic cycle of the enzyme. Although some models of the C-cluster of CODH nicely mimic the cuboidal [$NiFe_3S_4$] framework, all models reported so far are lacking the unique exo-Fe center. We showed that the {FeCp*Cl} fragment can be bound to a Ni(II)S_4 by bridging thiolates. Thereby, the combination of the strongly σ electron-donating Cp* ligand and the hard thiolate and chloride ligands stabilizes the high-spin state of iron. Therefore, the synthetic approach reported in this work may be used for integrating a high-spin Fe(II) into a [$NiFe_3S_4$] framework of a synthetic CODH model via bridging sulfides or thiolates. Finally, these examples clearly show us that nature has designed catalysts with complementary electronic structures for two quite different processes by fine-tuning the coordination geometry, ligands, and electronic structure of abundant metals like nickel and iron.

EXPERIMENTAL SECTION

Materials. All reactions were carried out under an inert atmosphere of argon using a dry argon glovebox (MBraun LabMaster130). THF used for chemical reactions and electrochemical measurements was dried over sodium with benzophenone and distilled under argon. *n*-Hexane used for crystallization was purified by the solvent purification system MBraun MB SPS-800 Auto. Ni precursors were synthesized according to the literature procedures.[54,55] The supporting electrolyte NBu_4BF_4 used for electrochemistry was purchased from Sigma-Aldrich and dried overnight at 100 °C under vacuum before use. Elemental analysis was performed on an Elementar Vario CHN-analyzer.

Spectroscopy. Absorption spectra were obtained using a diode-array ultraviolet−visible (UV−vis) spectrometer (HP 8453). Absorption spectra of samples prepared in an anaerobic chamber were measured in 1 cm path length cuvettes sealed with a silicon stopper to retain anaerobic conditions, and spectra were measured quickly (<2 min) after removing the samples from the anaerobic chamber to avoid decomposition. No changes in the absorption spectra were observed over the time scale of these measurements. Averages of three dilutions were considered to obtain accurate extinction coefficients considering only points within the linear range of the instrument (0.005−1 AU).

X-band EPR measurements were performed using a Bruker E500 ELEXSYS CW spectrometer with the Bruker dual-mode cavity (ER4116DM) and an Oxford Instruments helium-flow cryostat (ESR 910). For the EPR spectra (presented in the Supporting Information) MW frequencies of 9.6576 and 9.3974 GHz were used for perpendicular and parallel-modes, respectively.

Mössbauer spectra were recorded on a conventional spectrometer with alternating constant acceleration of the γ source. The minimum experimental line width was 0.24 mm/s (full width at half-height). The sample temperature was maintained constant in an Oxford Instruments Variox or in an Oxford Instruments Mössbauer-Spectromag cryostat with split-pair magnet system; the latter was used for measurements with applied field with the field at the sample being oriented perpendicular to the γ beam. The γ source (^{57}Co/Rh, 1.8 GBq) was kept at room temperature. By using a re-entrant bore tube the γ source could be positioned inside the gap of the magnet coils at a position with zero field. Isomer shifts are quoted relative to iron metal at 300 K. Mössbauer spectra at zero field were collected for powder samples (ca. 50 mg) at 80 K. The Mössbauer spectra recorded at zero field were fitted using the program MFIT (by E.B.) with Lorentzian doublets.

Magnetic Susceptibility Measurements. Magnetic susceptibility data were collected in the solid state or in THF solution (8 mmolar) in the temperature range of 2−300 K on a SQUID susceptometer (MPMS-7, Quantum Design) with a field of 1.0 T. The experimental data were corrected for underlying diamagnetism by use of tabulated Pascal's constants. The susceptibility data were simulated using the program julX (by E.B.). The formalism used for simulations is described in the Supporting Information.

Electrochemistry. All electrochemical measurements were carried out under argon atmosphere at room temperature using an EG&G

dx.doi.org/10.1021/ic500910z | Inorg. Chem. 2014, 53, 6329−6337

PAR 273A instrument. All solutions contained the supporting electrolyte NBu_4BF_4 (0.2 M in dichloromethane or acetonitrile). For cyclic voltammetry a standard three-electrode configuration was used consisting of a glassy carbon (d = 2 mm) working and counter-electrode and a Ag wire placed in a $AgNO_3$ (0.01 M in MeCN)/NBu_4PF_6 (0.2 M in MeCN) solution as a pseudoreference electrode. The system was systematically calibrated against ferrocene after each experiment, and all the potentials are therefore given versus the Fc/Fc^+ redox potential.

Crystal-Structure Analysis. Dark red single crystals **1**·1.5 THF, **2**, **3**, and **4**·0.5 THF were mounted on a Bruker-AXS Kappa Mach3 APEX-II diffractometer equipped with an Incoatec Helios mirror monochromator (Mo Kα λ = 0.710 73 Å) and a nitrogen cold stream adjusted to 100 K. Data were integrated and averaged with the program SAINT.[80] Final cell constants were obtained from least-squares fits of all measured reflections. An empirical absorption correction was performed using the Gaussian procedure embedded in SADABS.[81] The structures were readily solved by Patterson methods and subsequent difference Fourier techniques. The Siemens ShelXTL software package was used for solution and artwork of the structures; ShelXL97 was used for the refinement.[82,83] All non-hydrogen atoms were anisotropically refined. Hydrogen atoms bound to carbon were placed at calculated positions and refined as riding atoms with isotropic displacement parameters. The cyclohexyl rings in compounds **1**·1.5 THF and **2** as well as the solvent molecules in **1**·1.5 THF exhibit significant disorder. A split-atom model with restrained thermal displacement parameters and bond distances using EADP and SADI instructions in ShelXL97 was successfully used to account for this disorder.

Computational Methods. All calculations reported in this paper were performed using the ORCA program package.[84,85] Geometry optimizations were carried out at DFT level, using the BP86 generalized gradient approximations functional in conjunction with the resolution of identity approximation.[86−91] Initial atomic coordinates were taken from single-crystal X-ray diffraction experiments. We used the recontracted scalar-relativistic def2-TZVP basis set on all atoms, combined with the corresponding def2-TZVP/J auxiliary basis.[92−95] Stationary points were confirmed to be minima by the absence of imaginary frequencies. Final single-point energies were computed using the B3LYP hybrid functional with the accelerating RIJCOSX algorithm in conjunction with the def2-TZVP basis set.[96−99] The calculated quasi-restricted orbitals as well as the calculated spin density were visualized using the Chimera program.[100] Details for the computation of the Mössbauer parameters are given in the Supporting Information.

Synthesis of [Ni(xch)FeCp*Cl] 1. A suspension of Cp*Li (28 mg, 0.20 mmol) and $FeCl_2(THF)_{1.5}$ (47 mg, 0.2 mmol) in THF (3 mL) was stirred at −40 °C for 5 min until a green solution was obtained. [Ni(xch)] (91 mg, 0.2 mmol) was added as a solid, and the solution immediately turned red. The solution was allowed to warm to room temperature and stirred for 10 min. *n*-Hexane (1 mL) was added, and a white precipitate (LiCl) was filtered off. The red filtrate was overlaid by *n*-hexane (5 mL) and stored at −40 °C. The product was isolated as red crystals and dried under reduced pressure (60−67%). X-ray suitable crystals of **1**·1.5 THF were grown by the overlaying technique from THF and *n*-hexane at −40 °C. ^{57}Fe-Mössbauer (80 K, 0 T): δ = 1.07 mm/s, ΔE_Q = 2.53 mm/s. μ_{eff} (70−300 K) = 4.90 μ_B. Elemental analysis calculated for $C_{30}H_{43}FeNiClS_4$: C 52.84, H 6.36, Cl 5.20, found: C 50.66, H 6.08, Cl 5.31%. UV−vis (THF): λ (nm), ε (cm^{-1} mM^{-1}): 326 (11.6), 398 (4), 530 (1).

Complexes **2**−**4** were synthesized and purified in analogy to complex **1**.

[Ni(pdtch)FeCp*Cl] 2. ^{57}Fe-Mössbauer (80 K, 0 T): δ = 0.96 mm/s, ΔE_Q = 2.68 mm/s. μ_{eff} (70−300 K) = 5.08 μ_B. Elemental analysis calculated for $C_{25}H_{41}FeNiClS_4$: C 48.44, H 6.67, Cl 5.72, found: C 49.26, H 6.69, Cl 5.13%. UV−vis (THF): λ (nm), ε (cm^{-1} mM^{-1}): 315 (10.2), 339 (8.8), 520 (0.6).

[Ni(pdtdm)FeCp*Cl] 3. ^{57}Fe-Mössbauer (80 K, 0 T): δ = 1.08 mm/s, ΔE_Q = 2.53 mm/s. μ_{eff} (70−300 K) = 5.01 μ_B. Elemental analysis calculated for $C_{21}H_{37}FeNiClS_4$: C 44.42, H 6.57, Cl 6.24, found: C 43.16, H 6.58, Cl 5.68%. UV−vis (THF): λ (nm), ε (cm^{-1} mM^{-1}): 324 (7.9), 381 (2.8), 506 (0.7).

[Ni(xbsms)FeCp*Cl] 4. ^{57}Fe-Mössbauer (80 K, 0 T): δ = 1.07 mm/s, ΔE_Q = 2.63 mm/s. μ_{eff} (70−300 K) = 4.95 μ_B. Elemental analysis calculated for $C_{26}H_{39}FeNiClS_4$: C 49.58, H 6.24, Cl 5.63, found: C 49.26, H 6.69, Cl 5.13%. UV−vis (THF): λ (nm), ε (cm^{-1} mM^{-1}): 339 (7.2), 426 (1.9), 528 (0.9).

■ ASSOCIATED CONTENT

Ⓢ Supporting Information

Abbreviations, details on the analysis of SQUID data, Mössbauer calculations, and X-Band CW EPR spectra in parallel and perpendicular mode. This material is available free of charge via the Internet at http://pubs.acs.org.

■ AUTHOR INFORMATION

Corresponding Author

*E-mail: wolfgang.lubitz@cec.mpg.de. Phone: +49 208 306 3614. Fax: +49 208 306 3955.

Present Address

Stiftstr. 34−36, D-45470, Mülheim an der Ruhr.

Notes

The authors declare no competing financial interest.

■ ACKNOWLEDGMENTS

This work was supported by the Max Planck Society. We also thank the Fonds der Chemischen Industrie for the Doctoral Kekulé Fellowship (K.W.). I. Heise is gratefully acknowledged for synthetic support. We thank B. Mienert for help with the Mössbauer and A. Göbels for help with the SQUID measurements.

■ REFERENCES

(1) Groysman, S.; Holm, R. H. *Biochemistry* **2009**, *48*, 2310−2320.
(2) Vignais, P. M.; Billoud, B. *Chem. Rev.* **2007**, *107*, 4206−4272.
(3) Lubitz, W.; Ogata, H.; Rüdiger, O.; Reijerse, E. *Chem. Rev.* **2014**, *114*, 4081−4148.
(4) Volbeda, A.; Charon, M. H.; Piras, C.; Hatchikian, E. C.; Frey, M.; Fontecilla-Camps, J. C. *Nature* **1995**, *373*, 580−587.
(5) Volbeda, A.; Garcin, E.; Piras, C.; de Lacey, A. L.; Fernández, V. M.; Hatchikian, E. C.; Frey, M.; Fontecilla-Camps, J. C. *J. Am. Chem. Soc.* **1996**, *118*, 12989−12996.
(6) Albracht, S. P. J.; Graf, E. G.; Thauer, R. K. *FEBS Lett.* **1982**, *140*, 311−313.
(7) Surerus, K. K.; Chen, M.; van der Zwaan, J. W.; Rusnak, F. M.; Kolk, M.; Duin, E. C.; Albracht, S. P. J.; Münck, E. *Biochemistry* **1994**, *33*, 4980−4993.
(8) Pandelia, M. E.; Bykov, D.; Izsak, R.; Infossi, P.; Giudici-Orticoni, M. T.; Bill, E.; Neese, F.; Lubitz, W. *Proc. Nat. Ac. Sci. U.S.A.* **2013**, *110*, 483−488.
(9) Pierik, A. J.; Roseboom, W.; Happe, R. P.; Bagley, K. A.; Albracht, S. P. J. *J. Biol. Chem.* **1999**, *274*, 3331−3337.
(10) De Lacey, A. L.; Fernández, V. M.; Rousset, M.; Cammack, R. *Chem. Rev.* **2007**, *107*, 4304−4330.
(11) Lubitz, W.; Reijerse, E.; van Gastel, M. *Chem. Rev.* **2007**, *107*, 4331−4365.
(12) Ogata, H.; Lubitz, W.; Higuchi, Y. *Dalton Trans.* **2009**, 7577−7587.
(13) Lindahl, P. A. *J. Inorg. Biochem.* **2012**, *106*, 172−178.
(14) Kampa, M.; Pandelia, M. E.; Lubitz, W.; van Gastel, M.; Neese, F. *J. Am. Chem. Soc.* **2013**, *135*, 3915−3925.
(15) Canaguier, S.; Artero, V.; Fontecave, M. *Dalton Trans.* **2008**, 315−325.
(16) Tard, C.; Pickett, C. J. *Chem. Rev.* **2009**, *109*, 2245−2274.
(17) Ohki, Y.; Tatsumi, K. *Eur. J. Inorg. Chem.* **2011**, 973−985.

(18) Simmons, T. R.; Berggren, G.; Bacchi, M.; Fontecave, M.; Artero, V. *Coord. Chem. Rev.* **2014**, *270*−*271*, 127−150.
(19) Ohki, Y. *Bull.Chem. Soc. Jpn.* **2014**, *87*, 1−19.
(20) Li, Z.; Ohki, Y.; Tatsumi, K. *J. Am. Chem. Soc.* **2005**, *127*, 8950−8951.
(21) Jiang, J.; Maruani, M.; Solaimanzadeh, J.; Lo, W.; Koch, S. A.; Millar, M. *Inorg. Chem.* **2009**, *48*, 6359−6361.
(22) Tanino, S.; Li, Z.; Ohki, Y.; Tatsumi, K. *Inorg. Chem.* **2009**, *48*, 2358−2360.
(23) Lai, C. H.; Reibenspies, J. H.; Darensbourg, M. Y. *Angew. Chem., Int. Ed.* **1996**, *35*, 2390−2393.
(24) Osterloh, F.; Saak, W.; Haase, D.; Pohl, S. *Chem. Commun.* **1997**, 979−980.
(25) Davies, C.; Evans, J.; Hughes, L.; Longhurst, S.; Sanders, R. J. *Chem. Commun.* **1999**, 1935−1936.
(26) Liaw, W. F.; Chiang, C. Y.; Lee, G. H.; Peng, S. M.; Lai, C. H.; Darensbourg, M. Y. *Inorg. Chem.* **2000**, *39*, 480−484.
(27) Sellmann, D.; Geipel, F.; Lauderbach, F.; Heinemann, F. W. *Angew. Chem., Int. Ed.* **2002**, *41*, 632−634.
(28) Verhagen, J. A. W.; Lutz, M.; Spek, A. L.; Bouwman, E. *Eur. J. Inorg. Chem.* **2003**, *2003*, 3968−3974.
(29) Zhu, W.; Marr, A. C.; Wang, Q.; Neese, F.; Spencer, D. J. E.; Blake, A. J.; Cooke, P. A.; Wilson, C.; Schröder, M. *Proc. Natl. Acad. Sci. U.S.A.* **2005**, *102*, 18280−18285.
(30) Stenson, P. A.; Marin-Becerra, A.; Wilson, C.; Blake, A. J.; McMaster, J.; Schröder, M. *Chem. Commun.* **2006**, 317−319.
(31) Ohki, Y.; Yasumura, K.; Kuge, K.; Tanino, S.; Ando, M.; Li, Z.; Tatsumi, K. *Proc. Nat. Acad. Sci. U.S.A.* **2008**, *105*, 7652−7657.
(32) Barton, B. E.; Whaley, C. M.; Rauchfuss, T. B.; Gray, D. L. *J. Am. Chem. Soc.* **2009**, *131*, 6942−6943.
(33) Barton, B. E.; Rauchfuss, T. B. *J. Am. Chem. Soc.* **2010**, *132*, 14877−14885.
(34) Canaguier, S.; Field, M.; Oudart, Y.; Pécaut, J.; Fontecave, M.; Artero, V. *Chem. Commun.* **2010**, *46*, 5876−5878.
(35) Weber, K.; Krämer, T.; Shafaat, H. S.; Weyhermüller, T.; Bill, E.; van Gastel, M.; Neese, F.; Lubitz, W. *J. Am. Chem. Soc.* **2012**, *134*, 20745−20755.
(36) Ogo, S.; Ichikawa, K.; Kishima, T.; Matsumoto, T.; Nakai, H.; Kusaka, K.; Ohhara, T. *Science* **2013**, *339*, 682−684.
(37) Manor, B. C.; Rauchfuss, T. B. *J. Am. Chem. Soc.* **2013**, *135*, 11895−11900.
(38) Lindahl, P. A. *Biochemistry* **2002**, *41*, 2097−2105.
(39) Lindahl, P. A.; Graham, D. E. *Met. Ions Life Sci.* **2007**, 357−415.
(40) Dobbek, H.; Svetlichnyi, V.; Gremer, L.; Huber, R.; Meyer, O. *Science* **2001**, *293*, 1281−1285.
(41) Jeoung, J. H.; Dobbek, H. *Science* **2007**, *318*, 1461−1464.
(42) Kung, Y.; Drennan, C. L. *Curr. Opin. Chem. Biol.* **2011**, *15*, 276−283.
(43) Amara, P.; Mouesca, J. M.; Volbeda, A.; Fontecilla-Camps, J. C. *Inorg. Chem.* **2011**, *50*, 1868−1878.
(44) Hu, Z.; Spangler, N. J.; Anderson, M. E.; Xia, J.; Ludden, P. W.; Lindahl, P. A.; Münck, E. *J. Am. Chem. Soc.* **1996**, *118*, 830−845.
(45) Ralston, C. Y.; Wang, H.; Ragsdale, S. W.; Kumar, M.; Spangler, N. J.; Ludden, P. W.; Gu, W.; Jones, R. M.; Patil, D. S.; Cramer, S. P. *J. Am. Chem. Soc.* **2000**, *122*, 10553−10560.
(46) Gu, W.; Seravalli, J.; Ragsdale, S. W.; Cramer, S. P. *Biochemistry* **2004**, *43*, 9029−9035.
(47) Ciurli, S.; Ross, P. K.; Scott, M. J.; Yu, S. B.; Holm, R. H. *J. Am. Chem. Soc.* **1992**, *114*, 5415−5423.
(48) Zhou, J.; Scott, M. J.; Hu, Z.; Peng, G.; Münck, E.; Holm, R. H. *J. Am. Chem. Soc.* **1992**, *114*, 10843−10854.
(49) Zhou, J.; Raebiger, J. W.; Crawford, C. A.; Holm, R. H. *J. Am. Chem. Soc.* **1997**, *119*, 6242−6250.
(50) Panda, R.; Zhang, Y.; McLauchlan, C. C.; Rao, V. P.; Tiago de Oliveira, F. A.; Münck, E.; Holm, R. H. *J. Am. Chem. Soc.* **2004**, *126*, 6448−6459.
(51) Panda, R.; Berlinguette, C. P.; Zhang, Y.; Holm, R. H. *J. Am. Chem. Soc.* **2005**, *127*, 11092−11101.
(52) Sun, J.; Tessier, C.; Holm, R. H. *Inorg. Chem.* **2007**, *46*, 2691−2699.
(53) Wolf, R.; Schnöckelborg, E.-M. *Chem. Commun.* **2010**, *46*, 2832−2834.
(54) Verhagen, J. A. W.; Ellis, D. D.; Lutz, M.; Spek, A. L.; Bouwman, E. *Dalton Trans.* **2002**, 1275−1280.
(55) Weber, K.; Heise, I.; Weyhermüller, T.; Lubitz, W. *Eur. J. Inorg. Chem.* **2014**, 148−155.
(56) Oudart, Y.; Artero, V.; Pécaut, J.; Fontecave, M. *Inorg. Chem.* **2006**, *45*, 4334−4336.
(57) Canaguier, S.; Vaccaro, L.; Artero, V.; Ostermann, R.; Pécaut, J.; Field, M. J.; Fontecave, M. *Chem.—Eur. J.* **2009**, *15*, 9350−9364.
(58) Tilset, M.; Fjeldahl, I.; Hamon, J. R.; Hamon, P.; Toupet, L.; Saillard, J. Y.; Costuas, K.; Haynes, A. *J. Am. Chem. Soc.* **2001**, *123*, 9984−10000.
(59) Sitzmann, H.; Dezember, T.; Kaim, W.; Baumann, F.; Stalke, D.; Kärcher, J.; Dormann, E.; Winter, H.; Wachter, C.; Kelemen, M. *Angew. Chem., Int. Ed.* **1996**, *35*, 2872−2875.
(60) Sitzmann, H. *Coord. Chem. Rev.* **2001**, *214*, 287−327.
(61) Wallasch, M. W.; Rudolphi, F.; Wolmerhäuser, G.; Sitzmann, H. *Z. Naturforsch.* **2009**, *64b*, 11−17.
(62) Girerd, J.-J.; Journaux, Y. In *Physical Methods in Bioinorganic Chemistry*; Que, L. J., Ed.; University Science Books: Sausalito, CA, 2000; pp 321−374.
(63) Boca, R. *Coord. Chem. Rev.* **2004**, *248*, 757−815.
(64) Schulz, C.; Debrunner, P. *J. Phys. Colloq.* **1976**, *37*, C6−153.
(65) McLaughlin, M. P.; Retegan, M.; Bill, E.; Payne, T. M.; Shafaat, H. S.; Pena, S.; Sudhamsu, J.; Ensign, A. A.; Crane, B. R.; Neese, F.; Holland, P. L. *J. Am. Chem. Soc.* **2012**, *134*, 19746−19757.
(66) Solomon, E. I.; Lever, A. B. P. *Inorganic Electronic Structure and Spectroscopy;* John Wiley & Sons: New York, 2006.
(67) Hendrich, M. P.; Debrunner, P. G. *Biophys. J.* **1989**, *56*, 489−506.
(68) Surerus, K. K.; Hendrich, M. P.; Christie, P. D.; Rottgardt, D.; Orme-Johnson, W. H.; Münck, E. *J. Am. Chem. Soc.* **1992**, *114*, 8579−8590.
(69) Jang, H. G.; Hendrich, M. P.; Que, L. *Inorg. Chem.* **1993**, *32*, 911−918.
(70) Andres, H.; Bominaar, E. L.; Smith, J. M.; Eckert, N. A.; Holland, P. L.; Münck, E. *J. Am. Chem. Soc.* **2002**, *124*, 3012−3025.
(71) Krzystek, J.; Ozarowski, A.; Telser, J. *Coord. Chem. Rev.* **2006**, *250*, 2308−2324.
(72) Hans, M.; Buckel, W.; Bill, E. *J. Biol. Inorg. Chem.* **2008**, *13*, 563−574.
(73) Mathies, G.; Chatziefthimiou, S. D.; Maganas, D.; Sanakis, Y.; Sottini, S.; Kyritsis, P.; Groenen, E. J. J. *J. Magn. Reson.* **2012**, *224*, 94−100.
(74) Stathi, P.; Mitrikas, G.; Sanakis, Y.; Louloudi, M.; Deligiannakis, Y. *Mol. Phys.* **2013**, *111*, 2942−2949.
(75) Bencini, A.; Gatteschi, D. *EPR of Exchange Coupled Systems;* Springer: Berlin, Germany, 1990.
(76) Gütlich, P., Bill, E., Trautwein, A. X. *Mössbauer Spectroscopy and Transition Metal Chemistry. Fundamentals and Applications;* Springer: Heidelberg, Germany, 2011.
(77) Römelt, M.; Ye, S.; Neese, F. *Inorg. Chem.* **2008**, *48*, 784−785.
(78) Neese, F. *J. Am. Chem. Soc.* **2006**, *128*, 10213−10222.
(79) Ye, S.; Geng, C. Y.; Shaik, S.; Neese, F. *Phys. Chem. Chem. Phys.* **2013**, *15*, 8017−8030.
(80) *SAINT,* Version 7.46A; Bruker-AXS Inc.: Madison, WI, 2008.
(81) *SADABS,* Version 2009/1; Bruker-AXS Inc.: Madison, WI, 2009.
(82) *ShelXTL,* 2013/2; Bruker AXS Inc.: Madison, WI, 2013.
(83) Sheldrick, G. M. *ShelXL 2013,* University of Göttingen: Göttingen, Germany, 2013.
(84) Neese, F. *ORCA-Package,* Version 2.9.0; University of Bonn: Bonn, Germany, 2012.
(85) Neese, F. *WIREs Comput. Mol. Sci.* **2012**, *2*, 73−78.
(86) Becke, A. D. *Phys. Rev. A* **1988**, *38*, 3098−3100.
(87) Perdew, J. P. *Phys. Rev. B* **1986**, *33*, 8822−8824.

(88) Baerends, E. J.; Ellis, D. E.; Ros, P. *Chem. Phys.* **1973**, *2*, 41−51.
(89) Dunlap, B. I.; Connolly, J. W. D.; Sabin, J. R. *J. Chem. Phys.* **1979**, *71*, 3396−3403.
(90) Vahtras, O.; Almlöf, J.; Feyereisen, M. W. *Chem. Phys. Lett.* **1993**, *213*, 514−518.
(91) Neese, F. *J. Comput. Chem.* **2003**, *24*, 1740−1747.
(92) Pantazis, D. A.; Chen, X. Y.; Landis, C. R.; Neese, F. *J. Chem. Theory Comput.* **2008**, *4*, 908−919.
(93) Weigend, F. *Phys. Chem. Chem. Phys.* **2006**, *8*, 1057−1065.
(94) Eichkorn, K.; Treutler, O.; Öhm, H.; Häser, M.; Ahlrichs, R. *Chem. Phys. Lett.* **1995**, *240*, 283−290.
(95) Eichkorn, K.; Weigend, F.; Treutler, O.; Ahlrichs, R. *Theor. Chem. Acc.* **1997**, *97*, 119−124.
(96) Becke, A. D. *J. Chem. Phys.* **1993**, *98*, 5648.
(97) Stephens, P. J.; Devlin, F. J.; Chabalowski, C. F.; Frisch, M. J. *J. Phys. Chem.* **1994**, *98*, 11623−11627.
(98) Lee, C.; Yang, W.; Parr, R. G. *Phys. Rev. B* **1988**, *37*, 785−789.
(99) Neese, F.; Wennmohs, F.; Hansen, A.; Becker, U. *Chem. Phys.* **2009**, *356*, 98−109.
(100) Pettersen, E. F.; Goddard, T. D.; Huang, C. C.; Couch, G. S.; Greenblatt, D. M.; Meng, E. C.; Ferrin, T. E. *J. Comput. Chem.* **2004**, *25*, 1605−1612.

dx.doi.org/10.1021/ic500910z | *Inorg. Chem.* 2014, 53, 6329−6337